ADVANCED FUNCTIONAL MATERIALS
www.afm-journal.de

Chromaticity Control in Light-Emitting Electrochemical Cells via Thermally Activated Emission in Assemblies of a BN-Doped Pyrenyl Hydrocarbon

Luca M. Cavinato, Marco Franceschini, Laura Caputo, Jean-Christophe Charlier, Marc de Wergifosse, Davide Bonifazi, and Rubén D. Costa**

This work outlines the synthesis and photo-/electro-luminescent behavior of a new C-shaped BN-doped benzenoid hydrocarbon using N-directed borylation in a unique lattice-embedded graphitic C_2–B–N motif at the pyrene K-region. This BN-doped polycyclic aromatic hydrocarbon (PAH) exhibits a green fluorescent emission in solution with a photoluminescent quantum yield of 91%. In contrast, thin-films applied to light-emitting electrochemical cells (LECs) feature a temperature-dependent dual-emission, including a broad yellowish band and a well-structured near-infrared band that are barely met in the prior art. What is more striking, this temperature-dependent dual-emission can be easily controlled in LECs with the driving conditions, realizing green-yellow (*x/y* CIE color coordinates of 0.36/0.61; stabilities of 200 h; efficiency of 0.30 lm W^{-1}) and yellow-orange (*x/y* CIE color coordinates of 0.50/0.49; stabilities of ≈70 h; efficiency of 0.26 lm W^{-1}) devices. Finally, the expected greenish devices (*x/y* CIE color coordinates of 0.30/0.62; stabilities of 0.3 h; efficiency of 0.46 lm W^{-1}) can be fabricated using a host:guest active layer that disrupts the formation of the thermally activated emissive assemblies. Hence, this work highlights the films' thermally activated emission behavior to control device chromaticity using this BN-doped PAH.

1. Introduction

Light-emitting electrochemical cells (LECs) are emerging as a viable platform for efficient, solution-processed electroluminescent devices with a fair tolerance to shapes (forks, cables, *etc.*), electrodes, and thickness due to their simplified architecture, easy fabrication via spray-coating, and unique working mechanism.[1] These attributes make LECs promising candidates for low-cost and efficient lighting solutions for applications in signaling, decoration, medicine, etc.[2–5] Indeed, LECs exhibit moderate power efficiencies at low operating voltages by utilizing a single active layer comprising a blend of mobile ions and electroactive compounds. Upon applying a bias, ion polarization near the electrode interfaces forms electric double layers (EDLs), enabling charge injection to form doped layers that create a dynamic p-*i*-n junction. This results in efficient charge transport and recombination, producing stable luminance over time.[6–10]

Despite these advantages, the top-performing LECs are based on costly conjugated polymers[11,12] or rare metal complexes, such as Ir(III)-based complexes.[13–17] As a result, researchers are actively exploring alternative emitters. Notable progress has been made with Cu(I)-based complexes and small organic molecules as potential electroactive materials for LECs,[18–21] though each has distinct challenges: Cu(I)-based LECs have demonstrated brightness levels above 100 cd m^{-2}, but limited operational lifetimes of a few hours,[22–27] whereas small molecule-based LECs achieved higher

L. M. Cavinato, R. D. Costa
Technical University of Munich
Campus Straubing for Biotechnology and Sustainability
Chair of Biogenic Functional Materials
Schulgasse 22, 94315 Straubing, Germany
E-mail: ruben.costa@tum.de

The ORCID identification number(s) for the author(s) of this article can be found under https://doi.org/10.1002/adfm.202506703

DOI: 10.1002/adfm.202506703

M. Franceschini, D. Bonifazi
Department of Organic Chemistry
Faculty of Chemistry
University of Vienna
Währinger Straße 38, Vienna 1090, Austria
E-mail: davide.bonifazi@univie.ac.at

L. Caputo, J.-C. Charlier
Institute of Condensed Matter and Nanosciences
Université catholique de Louvain (UCLouvain)
Chemin des étoiles 8, Louvain-la-Neuve 1348, Belgium

M. de Wergifosse
Institute of Condensed Matter and Nanosciences
Université catholique de Louvain (UCLouvain)
Place Louis Pasteur 1, Louvain-la-Neuve 1348, Belgium

brightness (>500 cd m^{-2}) with similar lifetimes.[28–31] Thus, other families, such as quantum dots,[32] perovskite nanoparticles,[33,34] dendrimers,[10] carbon dots,[35–37] and polycyclic aromatic hydrocarbons (PAHs)[38,39] are slowly emerging.

PAHs scaffolds are generally well-suited for solution-processed devices.[40–43] They also exhibit high photoluminescence quantum yields (φ), good electrochemical and thermal stabilities, and ambipolar carrier mobilities. Finally, fine control of the optoelectronic features of PAHs could be achieved by heteroatom doping, where selected C═C bonds in the benzenoic structure are substituted with heteroatomic couples such as boron and nitrogen.[44] The BN doping enables tailoring of the photoluminescence and optoelectronic characteristics by utilizing the similar structural and electronic properties of the B—N bond compared to C═C bonds.[45–48] For instance, early studies on BN PAH have provided various molecular structures with tailored properties, including B_3N_3-coronenes,[49–51] B_3N_6-[4]triangulene,[52] BN-dibenzophenalenes,[53,54] BN-acenoacene derivatives,[55] and BN-pyrenyl derivatives.[56,57] These are, indeed, all favorable traits for lighting applications.[58–60] On one hand, OLEDs have extensively exploited BN-doped materials as narrowband deep-blue emitters, achieving EQE >30% at 1 000 cd m^{-2}.[61–64] On the other hand, seminal work in molecular graphenoid-based LECs has already demonstrated significant potential in the red-emitting region and even white LECs with BN-nanographene-like emitters.[38,39,65] In parallel, promising seminal work has also been performed about the implementation of narrowband BN-doped materials in LECs, however, only as guests in complex host matrices.[66–69]

Building on these promising findings, this work focuses on the synthesis and photo-/electro-luminescent behaviors of a novel BN-doped PAH with a specific structural extension at the K-region of a pyrene referred to here as C-shaped PAH, **C-BN** (**Scheme 1**). In solution, **C-BN** displays a strong green fluorescence (φ = 91%). In contrast, **C-BN**-based thin films undergo a thermally activated dual-emissive behavior attributed to the presence of assemblies with yellow and near-infrared (NIR) emission features. This behavior is also noted in **C-BN** LECs upon controlling the driving conditions that rule the working device temperatures, realizing well-performing green-yellow and yellow-orange emitting devices with stable x/y CIE color coordinates of 0.36/0.61 and 0.50/0.49 associated with stabilities of 200 h and ≈80 h as well as efficiencies of 0.30 and 0.26 lm W^{-1}, respectively. Finally, greenish devices (x/y CIE color coordinates of 0.30/0.62) can also be prepared using a host:guest active layer that disrupts the formation of supramolecular assemblies (stability of ≈0.3 h and efficiency of 0.46 lm W^{-1}). Overall, this work demonstrates the potential of a BN-PAH as an efficient and stable emitter for fabricating both white LECs[39,65] and rainbow single-component LECs by leveraging thermally induced emission in thin films.

2. Results and Discussion

2.1. Synthesis and Characterization of C-Shaped BN-Nanographenes

The synthesis of **C-BN** was conceived starting from an aminoacyl-functionalized pyrene precursor to be planarized with B atoms via an *N*-directed borylation procedure using BBr_3, following the synthetic approach previously developed by us[55] (Scheme 1a). A convergent synthetic approach using iodobiphenylamine **1** was exploited, where molecule **1** was prepared following our recent synthetic protocol.[55] Suzuki-Miyaura cross-coupling reaction between iodobiphenylamine **2** and pinacolboryl pyrene gave pivaloyl-protected pyrene derivative **3** in good yield (75%). Subsequent acid-catalyzed hydrolysis afforded corresponding free amines **4**, which were then equipped with mesityl (Mes) moieties as solubilizing groups via Buchwald-Hartwig cross-coupling to give intermediate **5** in excellent yield (87%). These intermediates were prepared and used as atropisomeric mixtures. Finally, **C-BN** was obtained in 61% yield at 200 °C in 1,2,4-trichlorobenzene (TCB) via *N*-directed borylation of **4** in the presence of an excess of BBr_3 (30 eq) followed by B-arylation with PhMgBr. Pyrene **C-BN** is soluble in most organic solvents, allowing its processability in preparing LECs–vide infra. The molecular structure was confirmed through spectroscopical characterization using one-dimensional and two-dimensional ^1H, ^{13}C, and ^{11}B NMR (**F**igures S1–S13, Supporting Information). Crystals suitable for X-ray diffraction analysis were obtained by vapor diffusion of MeOH to a toluene solution (Scheme 1b; Figure S14, Supporting Information), as well as Table S1 (Supporting Information). Since **C-BN** represents the first example of a lattice-embedded graphitic C_2-B-N motif exploiting the K-region of pyrene, it is interesting to highlight the bonding properties of this motif. While the B—N bond lengths are similar (1.418–1.424 Å) to those reported for 1,2-azaborine derivatives,[70–73] the B–C bond at the K-region of pyrene is significantly longer (1.561 Å) than the other B—C bonds in the scaffold (1.536–1.539 Å), suggesting a lower degree of delocalization for the former bond. The crystal structure also reveals an arched backbone, likely caused by steric hindrance between the *N*-Mes group, the pyrene core, and the crystal packing.[74] Given the presence of bulky Mes groups oriented nearly perpendicular to the molecular scaffold, the solid-state organization is predominantly governed by C—H···π interactions (3.392–3.810 Å) with a minimal contribution given by weak π–π stacking contacts (3.484–3.541 Å) established among antiparallel pyrene cores.

2.2. Photophysical and Electrochemical Properties of C-BN in Solution

The UV-Vis absorption spectrum of **C-BN** was recorded in anhydrous 2-MeTHF at room temperature (**Figure 1a**) and shows three well-defined bands. In short, the low-energy and well-structured absorption band peaking at 441, 470, and 501 nm is associated with an absorption extinction coefficient (ϵ_{max}) of ≈61,500 M^{-1} cm^{-1}. Density functional theory (DFT) calculations and its time-dependent version (TD-DFT) using the B3LYP exchange-correlation functional and the 6–311G(d) basis set were carried out (see Supporting Information for more details). They indicate that this band is related to an electronic transition from the highest-occupied molecular orbital (HOMO) to the lowest-unoccupied molecular orbital (LUMO), defining a $\pi \rightarrow \pi^*$ transition that expands across the pyrene-B-N moieties (Figure 1b; Figures S15, S16 and Tables S2, S3 Supporting Information).

Upon excitation of the **C-BN** solutions at 470 nm, a bright and well-structured green emission peaking at 507, 544, 588, and

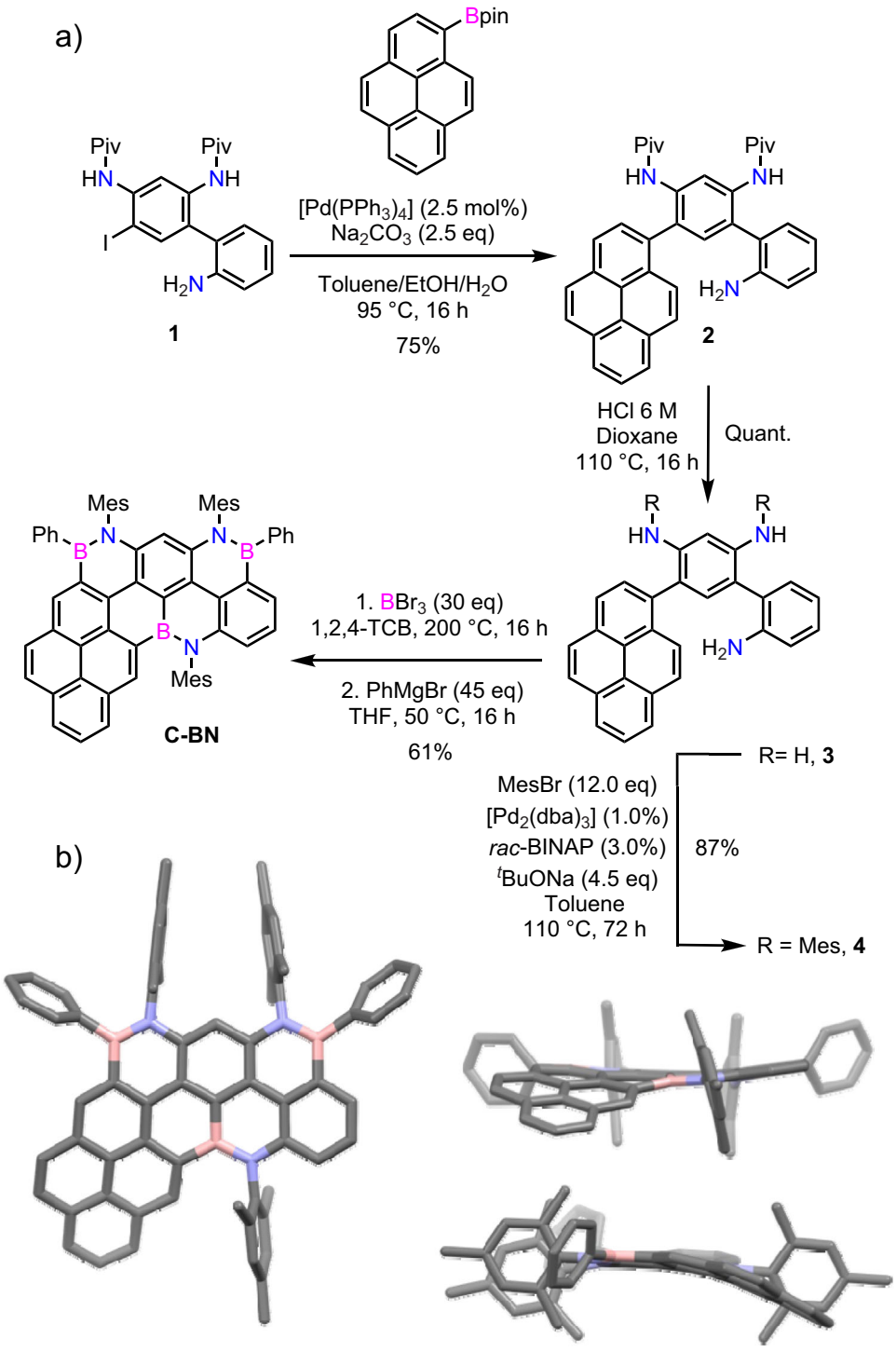

Scheme 1. a) Synthetic route to prepare **C-BN**; b) Single-crystal X-ray structures (carbon, nitrogen, and boron atoms are colored gray, blue, and pink, respectively, space group: *P*-1).

640 nm was noted(Figure 1a). This is associated with φ values of 91% and excited state lifetimes (τ) of 5.0 ns, indicating an intense fluorescence mechanism. In line with the UV–vis absorption profile, TD-DFT calculations suggest that this emission is attributed to the radiative relaxation of the lowest singlet excited state (HOMO→LUMO) transition with an estimated vertical energy of 503 nm. At 77 K, the well-structured emission holds without evolving any phosphorescence signal (Figure 1a). Indeed, calculations using different functionals and theoretical approaches showed that the energy splitting between the lowest excited S_1

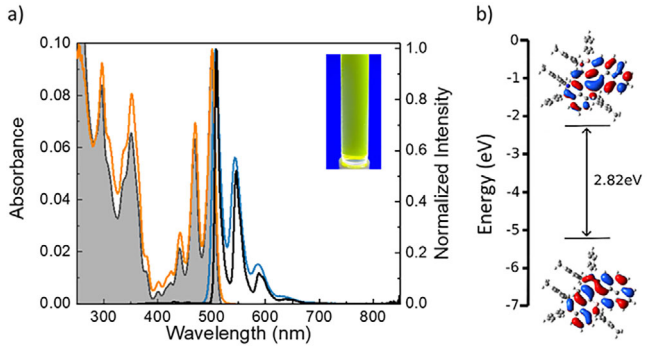

Figure 1. a) Absorption (gray), excitation (orange), and emission spectra at room temperature (blue) and at 77 K (black) of **C-BN** in 2-MeTHF solution. The inset shows the solution color under a UV lamp (λ_{exc} of 302 nm). b) The HOMO/LUMO of **C-BN** are mapped with an isosurface value of 0.02 e Å^{-3} with their respective bandgap. The positive and negative values of the electronic wavefunctions are depicted in blue and red, respectively.

and T_1 states ($\Delta E_{S\text{-}T}$) is ≈0.96 eV (Table S4, Supporting Information) and related discussion, indicating that thermally activated delayed fluorescence mechanism is not possible in **C-BN** at room temperature.

Finally, cyclic voltammetry (CV) experiments were carried out[55] (Figures S17, S18, Supporting Information). **C-BN** shows a one-electron reversible oxidation process at $E^{ox}_{1/2}$ = 0.96 V versus DmFc/DmFc$^+$ (0.41 V vs Fc/Fc$^+$). Notably, no reduction processes were observed in the given solvent. Thus, the HOMO energy level of −5.21 eV was experimentally determined from the $E^{ox}_{1/2}$. In contrast, the LUMO energy level of −2.79 eV was estimated using the optical bandgap ΔE_g^{opt} of 2.42 eV-see Supporting Information for further details.

2.3. Photo-/Electro-Luminescent Features of C-BN in Thin Films and Devices

Pristine and ion-doped (i.e., a blend of **C-BN** with tetrahexylammonium tetrafluoroborate (THA) in mass ratio 1:0.2 as used as active layer in LECs) thin-films were prepared with **C-BN** using spin-coating on quartz substrates. In general, atomic force microscopy (AFM) assays confirm that the thin films show smooth and homogenous morphologies with root-mean-square roughness of ≈500 pm, indicating the absence of large aggregates (Figure S19, Supporting Information). However, the emission spectrum at λ_{exc} of 440 nm shows a broad yet structured emission band centered at 585–600 nm regardless of the film composition (**Figure 2a**), displaying an almost 100 nm red-shifted compared to the emission in solution. This suggests the formation of supramolecular assemblies due to short-range interactions between **C-BN** molecules upon film forming. Indeed, adding long-alkyl chain ions, i.e., THA, partially disrupts these assemblies, as depicted by a second emission peak centered at 509 nm. Nonetheless, both φ and $<\tau>$ values are strongly reduced to 12%/19% and <1 ns/1.1 ns for pristine/ion-doped films, respectively. This suggests the presence of an effective aggregation-induced quenching.[75] To further support this hypothesis, the dispersion of **C-BN** in polystyrene (PS) matrix (1% wt.; **C-BN@PS**) films leads to the recovery of the well-structured emission expected from solution as well as enhanced photoluminescence figures-of-merit (i.e., φ of 63% and $<\tau>$ of 4.7 ns) (**Table 1**). Finally, also the dispersion of **C-BN** in an electroactive polymeric matrix (**C-BN@EP**, vide infra) led to the expected green-emitting films (i.e., φ of 48% and $<\tau>$ of 4.7 ns). Here, the exciplex formed by the blend's components and with emission maximum centered at 430 nm is also present[76] (Figure 2a).

Next, devices were fabricated by spin-coating the ion-doped active layer on glass/ITO/PEDOT:PSS substrates and finalized by evaporating Al cathode onto the active layer−see Supporting Information for further details. Initially, **C-BN**-LECs were driven at pulsed currents of 50 mA cm^{-2} based on a block wave at 1 kHz and a duty cycle of 50%, monitoring the luminance, color, and electrical behavior over time.[77] In detail, the devices showed the typical LEC behavior: an initial voltage (3.3 V) that exponentially reduces to a plateau ≈2.5 V. At the same time, the luminance rises from an initial value of 16 cd m^{-2} to a maximum of 27 cd m^{-2} (Figure 2b). The quick (<10 min) decrease in the average voltage is related to the electrochemical doping promoted by the formation of electrochemical double layers at the electrode interface. In contrast, the lack of a stable voltage plateau indicates a slow electrochemical degradation –, i.e., over-oxidation/reduction processes.[30] Indeed, a gradual drop in the luminance level was recorded, while the average voltage was continuously raised, ending up in a device lifetime of ≈80 h−$t_{1/2}$; time to reach half of the maximum luminance. Nevertheless, much more interesting than the device performance is the electroluminescent spectrum consisting of a broad emission centered at 600 nm and a well-structured emission band located at ≈760 nm (Figure 2c). This resulted in an orange emission associated with x/y CIE color coordinates of 0.50/0.49. Notably, no substantial shifts in the electroluminescence spectra and/or device chromaticity over the device lifespan were noted (Figure 2c).

While the yellow emission band is expected from the photoluminescence characterization – vide supra, the nature of the excited state involved in the low-energy electroluminescence band of **C-BN** is puzzling. In addition, the lack of color corruption over time excludes classical reasons, such as *i*) unbalanced doping and dynamic changes of the position of the emitting p–*i*–n junction,[78–80] *ii*) changes in the local electric field distribution and intensity as the voltage continuous rises,[30,39,65] and *iii*) microcavity and scattering effects.[81–83] Building on previous results of BN-nanographene emitters in LECs, the origin of the low-energy emission band could be related to the presence of lower-energy emitting species of **C-BN** assemblies that feature a thermally induced emissive behavior, as the LEC's operation temperature can reach values as high as 70 °C.[38,39,65]

To corroborate this hypothesis, we first investigated the temperature-dependent photoluminescence behavior from 77 to 500 K of the pristine **C-BN**-based films (Figure 2d,f; Figure S20, Supporting Information) and those blending 1 wt.% **C-BN** in PS (**C-BN@PS**) (Figure 2e,f; Figure S20, Supporting Information). At 77 K, pristine **C-BN** films already showed a broad yellow emission centered at 576 nm associated with a $<\tau>$ value of 2.6 ns. Upon heating up to 300 K, the λ_{max} gradually red-shifts to 600 nm, while $<\tau>$ values are linearly reduced. In contrast, **C-BN@PS** films show a well-structured emission that resembles the one recorded in 2-MeTHF at 77 K with $<\tau>$ values of 4.3 ns. Upon heating beyond 300 K, pristine **C-BN** films showed new

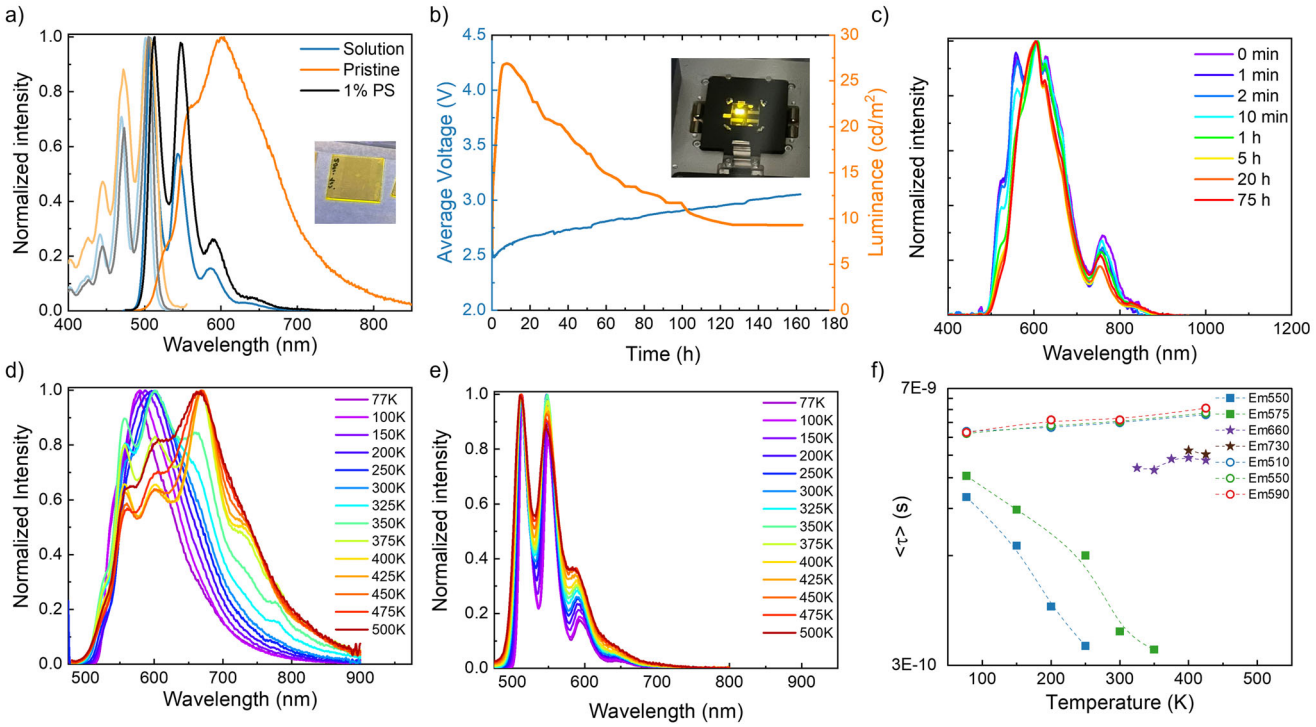

Figure 2. a) Emission spectra of **C-BN** solutions (purple) and **C-BN**-based thin-films of different compositions. Inset: picture of **C-BN**-based active layer under UV lamp (λ_{exc} = 365 nm). b) Luminance and applied average voltage over time of **C-BN**-based LECs driven at 50 mA cm^{-2} current compliance. c) Electroluminescent spectra change over time, highlighted by representative spectra taken at different times (see legend). d,e) Photoluminescence spectra (λ_{exc} = 473 nm) of **C-BN** pristine thin-films d) and **C-BN@PS** e) on quartz upon heating from 77 to 500 K. f) Average excited state lifetimes at different temperatures and at different emission wavelength (solid symbols refer to **C-BN** and empty symbols refer to **C-BN@PS** for reference purposes).

peaks centered at 660 and 730 nm. They exhibited a $<\tau>$ ≈3 ns that does not decrease upon heating. In contrast, **C-BN@PS** films show a gradual decrease in intensity without any change in the emission response (Figure 2e). Therefore, we conclude that the low-energy emission must be related to temperature-induced short-range molecular ordering or pairing (e.g., dimer or trimer species formation) and/or domain conformations in thin films that feature a thermally activated emission in the NIR region.[39] Finally, to exclude the presence of degradative species upon thermal treatment, the PL response of the used thin films of **C-BN** was recorded upon cooling at room temperature. No changes were noted (Figure S21, Supporting Information), highlighting the great thermal stability of this **C-BN** up to 500 K.

To carry out a similar temperature-dependent EL response, **C-BN**-based LECs were driven at current compliance of 20 and 150 mA cm^{-2}, reaching *in-operando* temperatures of 32 and 47 °C, respectively (Figure S22, Supporting Information). At 20 mA cm^{-2}, LECs exhibited moderate luminance (L_{max} 11 cd m^{-2}) with an outstanding stability of 200 h (Figure S23, Supporting Information) and **Table 2**. Here, the initial electroluminescence emission band resembles that of the solution with a well-structured band corresponding to a yellowish-green color with x/y CIE color coordinates of 0.36/0.61. The low-energy peak weakly evolves over the first minutes at which the device's temperature rises up to its maximum working temperature (Figure S22, Supporting Information). At 150 mA cm^{-2}, the devices feature a higher luminance (35 cd m^{-2}) and good stability ($t_{1/2}$ ≈80 h) (**Figure 3a** and Table 2).[28–30] Noteworthy, the electroluminescence emission band exhibited instantaneous and intense (up to 50% of the main peak intensity) low-energy peaks

Table 1. Photophysical properties of **C-BN**-based thin-films. The solution data are also reported as references.

State	Additives	λ_{em} [nm]	Φ [%]	$<\tau>$ [ns]	k_{rad} [×10^7 s^{-1}]	k_{nrad} [×10^7 s^{-1}]
Solution	–	507, 544, 588	91	5.0	18.2	1.8
Thin films	–	600	12	<1	39.7	291
	20% wt. THA	509, 585	19	1.1	17.0	72.6
	C-BN@PS	511, 547, 591	63	4.7	13.4	7.8
	C-BN@EP	430, 513, 551, 590	48	4.7	9.9	11.2

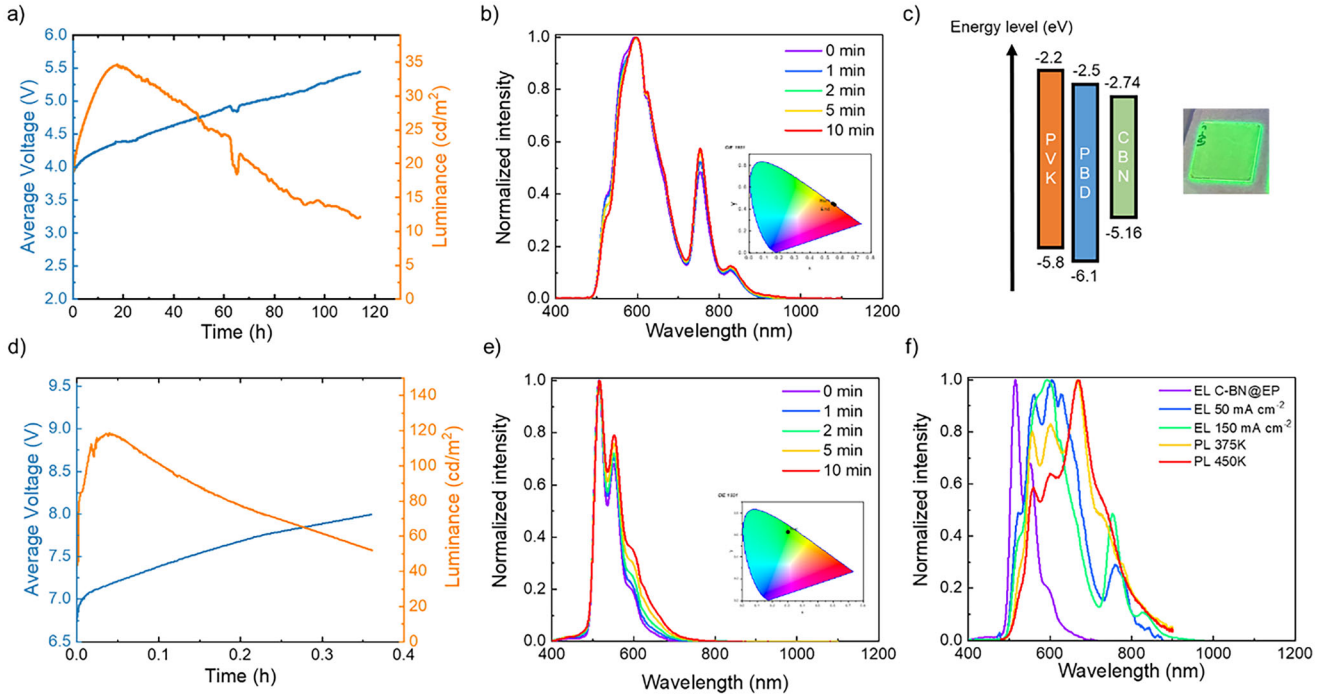

Figure 3. Luminance, applied average voltage, and electroluminescent changes of **C-BN-** a,b) and **C-BN@EP-**based (d-e) LECs driven at 150 mA cm^{-2} current compliance over time. The insets show the corresponding x/y CIE color coordinates. c) Energy levels diagram of the host materials PVK and PBD, and the guest emitter **C-BN**. The inset shows a picture of the active layer under UV-lamp (λ_{exc} = 365 nm). f) Comparison of the photoluminescence spectra of **C-BN** pristine thin films at different temperatures (see legend) and the EL spectra of **C-BN** based LECs at difference current compliance and **C-BN@EP** LECs at 150 mA cm^{-2}.

at 760 and 830 nm over the whole device lifespan (Figure 3b). This led to intense orange emission (x/y CIE color coordinates of 056/0.44).

Since the formation of short-range assemblies is related to the pair of statistically independent **C-BN** molecules, the device chromaticity should be highly sensitive to the emitter concentration. Thus, final confirmation came from devices in which **C-BN** is dispersed in an electroactive polymeric matrix (**C-BN@EP**) made of polyvinilcarbazole (PVK) and 2-(4-biphenyl)-5-(4-*tert*-butylphenyl)-1,3,4-oxadiazole (PBD) and the above ion-electrolyte to achieve a final active layer composition of PVK:PBD:**C-BN**:THA 1:1:0.16:0.08 mass ratio,—see SI for further details.[28] Here, the HOMO and LUMO of **C-BN** are above those one of PVK and below the one of PBD (Figure 3c). At the same time, the excitation spectrum of **C-BN** perfectly matches the electroluminescence response of the exciplex PVK:PBD, allowing optimal energy transfer (Figure S24, Supporting Information). At 150 mA cm^{-2}, LECs containing **C-BN@EP** featured an instantaneous luminescence of 40 cd m^{-2} that quickly rises, reaching a maximum of 120 cd m^{-2} (Figure 3d and Table 2). Furthermore, the electroluminescence spectrum entirely resembled the photoluminescence profile of highly diluted **C-BN@PS** films, resulting in a greenish device associated with x/y CIE color coordinates of 0.30/0.62 (Figure 3e). Here, the low-energy peak over the entire device lifespan is not present, though the working temperature is similar to the above single-component devices—vide supra. Unfortunately, the device stability is strongly reduced by the limited stability of the PVK:PBD layer at such applied current densities (Figure S25, Supporting Information).

Overall, these studies highlighted a correlation between the PL emission of C-BN-based thin films at 375 and 450 K (Figure 3f, yellow and red solid lines) and EL spectra of LECs drove at current compliance (Figure 3f, blue and green solid lines).

Table 2. Figures-of-merit of traditional LECs at different pulsed current driving and embedding different active layers.

Active Layer	Current density [mA cm^{-2}]	L_{max} [cd m^{-2}]	$t_{1/2}$ [h]	Efficiency [lm W^{-1}]	x/y CIE coordinates
C-BN	20	10.1 ± 0.74	191.2 ± 9.57	0.30 ± 0.027	0.36/0.61
	50	25.4 ± 1.14	72.3 ± 2.4	0.26 ± 0.011	0.50/0.49
	150	33.4 ± 1.30	74.4 ± 4.5	0.065 ± 0.005	0.56/0.44
C-BN@EP	150	111 ± 7.4	0.31 ± 0.05	0.46 ± 0.016	0.30/0.62

3. Conclusion

This work discusses the design, synthesis, and photo-/electroluminescent behaviors of a new pyrene-based BN-doped PAH, which exhibits unique features, such as *i*) an unprecedented structural motif with a planar graphitic C_2-N-B moiety bound to the pyrene K-region, *ii*) a bright green fluorescence associated to φ of 91% and reversible electrochemistry in solution, and *iii*) distinct temperature-dependent photoluminescence in thin-films and electroluminescence in LECs attributed to thermally activated NIR-emitting species. What is more interesting is that the temperature dependent emission from the supramolecular assemblies can be easily controlled with the operating conditions (i.e., working temperature) as well as the active layer composition (i.e., host:guest), going all the way from greenish (x/y CIE color coordinates of 0.30/0.62) to yellow-green (x/y CIE color coordinates of 0.36/0.61), and to yellow-orange (x/y CIE color coordinates of 0.50/0.49) devices. These color features are stable over the whole lifespan with a good device performance for the green/yellow/orange-emitting LECs. Compared to the prior literature in BN-emitters that show multiresonance and/or TADF emission mechanisms,[55,84] our BN-design turns out to be unique to tune device chromaticity in single-component and host:guest LECs by exploiting their thermally induced emission in thin-films.[39,65–69] However, device efficiency is limited by the nature of the emission of these C-BN emitters and the unclear role of low-energy emitting species. Currently, we are working on shedding more light onto the nature of the excited states and emitting species by ultra-fast time-resolved transient spectroscopy as well as how to enhance this photo-/electro-luminescent further to develop long-living and easy-to-prepare white and rainbow LECs based on newly devised BN-doped PAHs, including molecular graphenes.

Supporting Information

Supporting Information is available from the Wiley Online Library or from the author.

Acknowledgements

L.M.C., M.F., and L.C. contributed equally to this work. L.M.C., R.D.C., M.F., D.B., L.C., and J.C.C. acknowledge the European Union's Horizon 2020 MSCA-ITN (STiBNite, Contract No. 956923). L.C. thanks the UCLouvain "Fonds Spéciaux de Recherche" (FSR 2023) for additional PhD funding. The Computational resources have been provided by the CISM supercomputing facilities of UCLouvain and the CÉCI consortium funded by F.R.S.-FNRS of Belgium (N° 2.5020.11). D.B. and M.F. thank M. Crosta and R. R. Ferreira for single-crystal X-ray diffraction analysis and in-solution optoelectronic characterization. D.B. thanks the University of Vienna for generous funding.

Conflict of Interest

The authors declare no conflict of interest.

Data Availability Statement

The data that support the findings of this study are available from the corresponding author upon reasonable request.

Keywords

BN-doped polycyclic aromatic hydrocarbons, device chromaticity control, light-emitting electrochemical cells, pyrene, thermally activated emission

Received: March 15, 2025
Revised: July 21, 2025
Published online:

[1] a) E. Fresta, R. D. Costa, *J. Mater. Chem. C* **2017**, *5*, 5643; b) Q. Pei, R. D. Costa, *Adv. Funct. Mater.* **2020**, *30*, 2002879.
[2] E. Fresta, R. D. Costa, *Adv. Funct. Mater.* **2020**, *30*, 1908176.
[3] A. Sandström, L. Edman, *Energy Technol.* **2015**, *3*, 329.
[4] K. G. Cho, J. I. Lee, S. Lee, K. Hong, M. S. Kang, K. H. Lee, *Adv. Funct. Mater.* **2020**, *30*, 1907936.
[5] K. Schlingman, Y. Chen, R. S. Carmichael, T. B. Carmichael, *Adv. Mater.* **2021**, *33*, 2006863.
[6] K. Youssef, Y. Li, S. O'Keeffe, L. Li, Q. Pei, *Adv. Funct. Mater.* **2020**, *30*, 1909102.
[7] J. Fang, Y. Yang, L. Edman, *Appl. Phys. Lett.* **2008**, *93*, 063503.
[8] A. Munar, A. Sandström, S. Tang, L. Edman, *Adv. Funct. Mater.* **2012**, *22*, 1511.
[9] S. B. Meier, D. Tordera, A. Pertegás, C. Roldán-Carmona, E. Ortí, H. J. Bolink, *Mater. Today* **2014**, *17*, 217.
[10] L. M. Cavinato, K. Yamaoka, S. Lipinski, V. Calvi, D. Wehenkel, R. van Rijn, K. Albrecht, R. D. Costa, *Adv. Funct. Mater.* **2023**, *33*, 2302483.
[11] A. Asadpoordarvish, A. Sandström, S. Tang, J. Granström, L. Edman, *Appl. Phys. Lett.* **2012**, *100*, 193508.
[12] S. Tang, J. Pan, H. Buchholz, L. Edman, *ACS Appl. Mater. Interfaces* **2011**, *3*, 3384.
[13] J. D. Slinker, A. A. Gorodetsky, M. S. Lowry, J. Wang, S. Parker, R. Rohl, S. Bernhard, G. G. Malliaras, *J. Am. Chem. Soc.* **2004**, *126*, 2763.
[14] H. J. Bolink, E. Coronado, R. D. Costa, E. Ortí, M. Sessolo, S. Graber, K. Doyle, M. Neuburger, C. E. Housecroft, E. C. Constable, *Adv. Mater.* **2008**, *20*, 3910.
[15] S. Tang, A. Sandström, P. Lundberg, T. Lanz, C. Larsen, S. van Reenen, M. Kemerink, L. Edman, *Nat. Commun.* **2017**, *8*, 1190.
[16] R. D. Costa, G. Fernández, L. Sánchez, N. Martín, E. Ortí, H. J. Bolink, *Chem. – Eur. J.* **2010**, *16*, 9855.
[17] R. D. Costa, E. Ortí, H. J. Bolink, S. Graber, C. E. Housecroft, M. Neuburger, S. Schaffner, E. C. Constable, *Chem. Commun.* **2009**, 2029.
[18] K. Matsuki, J. Pu, T. Takenobu, *Adv. Funct. Mater.* **2020**, *30*, 1908641.
[19] C. E. Housecroft, E. C. Constable, *J. Mater. Chem. C* **2022**, *10*, 4456.
[20] G. U. Mahoro, J. Fernandez-Cestau, J. Renaud, P. B. Coto, R. D. Costa, S. Gaillard, *Adv. Opt. Mater.* **2020**, *8*, 2000260.
[21] A. Farokhi, S. Lipinski, L. M. Cavinato, H. Shahroosvand, B. Pashaei, S. Karimi, S. Bellani, F. Bonaccorso, R. D. Costa, *Chem. Soc. Rev.* **2025**, *54*, 266.
[22] L. M. Cavinato, S. Wölfl, A. Pöthig, E. Fresta, C. Garino, J. Fernandez-Cestau, C. Barolo, R. D. Costa, *Adv. Mater.* **2022**, *34*, 2109228.
[23] E. Fresta, M. D. Weber, J. Fernandez-Cestau, R. D. Costa, *Adv. Opt. Mater.* **2019**, *7*, 1900830.
[24] M. Elie, M. D. Weber, F. Di Meo, F. Sguerra, J.-F. Lohier, R. B. Pansu, J. L. Renaud, M. Hamel, M. Linares, R. D. Costa, S. Gaillard, *Chem. Eu. J.* **2017**, *23*, 16328.
[25] C. Li, C. F. R. Mackenzie, S. A. Said, A. K. Pal, M. A. Haghighatbin, A. Babaei, M. Sessolo, D. B. Cordes, A. M. Z. Z. Slawin, P. C. J. J. Kamer, H. J. Bolink, C. F. Hogan, E. Zysman-Colman, *Inorg. Chem.* **2021**, *60*, 10323.

[26] S. Keller, A. Pertegás, G. Longo, L. Martínez, J. Cerdá, J. M. Junquera-Hernández, A. Prescimone, E. C. Constable, C. E. Housecroft, E. Ortí, H. J. Bolink, *J. Mater. Chem. C* **2016**, *4*, 3857.
[27] M. D. Weber, E. Fresta, M. Elie, M. E. Miehlich, J.-L. Renaud, K. Meyer, S. Gaillard, R. D. Costa, *Adv. Funct. Mater.* **2018**, *28*, 1707423.
[28] P. Lundberg, Y. Tsuchiya, E. M. Lindh, S. Tang, C. Adachi, L. Edman, *Nat. Commun.* **2019**, *10*, 5307.
[29] S. Tang, P. Lundberg, Y. Tsuchiya, J. Ràfols-Ribé, Y. Liu, J. Wang, C. Adachi, L. Edman, *Adv. Funct. Mater.* **2022**, *32*, 2205967.
[30] M. D. Weber, M. Adam, R. R. Tykwinski, R. D. Costa, *Adv. Funct. Mater.* **2015**, *25*, 5066.
[31] S. Tang, Z. Wang, Y. Xu, H. Ma, J. Wang, C. Larsen, D. Dang, E. Wang, L. Edman, *Angew. Chem., Int. Ed.* **2023**, *62*, 202302874.
[32] E. Nannen, J. Frohleiks, S. Gellner, *Adv. Funct. Mater.* **2020**, *30*, 1907349.
[33] A. Mishra, S. DiLuzio, M. Alahbakhshi, A. C. Adams, M. H. Bowler, J. Moon, Q. Gu, A. A. Zakhidov, S. Bernhard, J. D. Slinker, *Chem. Mater.* **2021**, *33*, 1201.
[34] A. Mishra, R. Bose, Y. Zheng, W. Xu, R. McMullen, A. B. Mehta, M. J. Kim, J. W. P. Hsu, A. V. Malko, J. D. Slinker, *Adv. Mater.* **2022**, *34*, 2203226.
[35] Y. Liu, S. Tang, X. Wu, N. Boulanger, E. Gracia-Espino, T. Wågberg, L. Edman, J. Wang, *Nano Res.* **2022**, *15*, 5610.
[36] S. Tang, Y. Liu, H. Opoku, M. Gregorsson, P. Zhang, E. Auroux, D. Dang, A.-V. Mudring, T. Wågberg, L. Edman, J. Wang, *Green Chem.* **2023**, *25*, 9884.
[37] L. M. Cavinato, V. Kost, S. Campos-Jara, S. Ferrara, S. Chowdhury, I. M. Groot, T. Da Ros, R. D. Costa, *Adv. Opt. Mater.* **2024**, *12*, 2400618.
[38] E. Fresta, K. Baumgärtner, J. Cabanillas-Gonzalez, M. Mastalerz, R. D. Costa, *Nanoscale Horiz.* **2020**, *5*, 473.
[39] E. Fresta, J. Dosso, J. Cabanillas-González, D. Bonifazi, R. D. Costa, *Adv. Funct. Mater.* **2020**, *30*, 1906830.
[40] B. Kohl, F. Rominger, M. Mastalerz, *Chem. – Eur. J.* **2015**, *21*, 17308.
[41] B. Kohl, F. Rominger, M. Mastalerz, *Angew. Chem., Int. Ed.* **2015**, *54*, 6051.
[42] H. Seyler, B. Purushothaman, D. J. Jones, A. B. Holmes, W. W. H. Wong, *Pure Appl. Chem.* **2012**, *84*, 1047.
[43] Y. Zhong, B. Kumar, S. Oh, M. T. Trinh, Y. Wu, K. Elbert, P. Li, X. Zhu, S. Xiao, F. Ng, M. L. Steigerwald, C. Nuckolls, *J. Am. Chem. Soc.* **2014**, *136*, 8122.
[44] X.-Y. Wang, X. Yao, A. Narita, K. Müllen, *Acc. Chem. Res.* **2019**, *52*, 2491.
[45] Z. Liu, T. B. Marder, *Angew. Chem., Int. Ed.* **2008**, *47*, 242.
[46] M. J. D. Bosdet, W. E. Piers, *Can. J. Chem.* **2009**, *87*, 8.
[47] X.-Y. Wang, J.-Y. Wang, J. Pei, *Chem. – Eur. J.* **2015**, *21*, 3528.
[48] J. Huang, Y. Li, *Front. Chem* **2018**, *6*, 341.
[49] J. Dosso, J. Tasseroul, F. Fasano, D. Marinelli, N. Biot, A. Fermi, D. Bonifazi, *Angew. Chem., Int. Ed.* **2017**, *56*, 4483.
[50] M. Krieg, F. Reicherter, P. Haiss, M. Ströbele, K. Eichele, M.-J. Treanor, R. Schaub, H. F. Bettinger, *Angew. Chem., Int. Ed.* **2015**, *54*, 8284.
[51] J. Dosso, T. Battisti, B. D. Ward, N. Demitri, C. E. Hughes, P. A. Williams, K. D. M. Harris, D. Bonifazi, *Chem. – Eur. J.* **2020**, *26*, 6608.
[52] M. Zhao, Q. Miao, *Angew. Chem., Int. Ed.* **2021**, *60*, 21289.
[53] X. Wang, F. Zhang, K. S. Schellhammer, P. Machata, F. Ortmann, G. Cuniberti, Y. Fu, J. Hunger, R. Tang, A. A. Popov, R. Berger, K. Müllen, X. Feng, *J. Am. Chem. Soc.* **2016**, *138*, 11606.
[54] M. Numano, N. Nagami, S. Nakatsuka, T. Katayama, K. Nakajima, S. Tatsumi, N. Yasuda, T. Hatakeyama, *Chem.-Eur. J.* **2016**, *22*, 11574.
[55] M. Franceschini, M. Crosta, R. R. Ferreira, D. Poletto, N. Demitri, J. P. Zobel, L. González, D. Bonifazi, *J. Am. Chem. Soc.* **2022**, *144*, 21470.
[56] T. Hatakeyama, S. Hashimoto, S. Seki, M. Nakamura, *J. Am. Chem. Soc.* **2011**, *133*, 18614.
[57] S. Oda, K. Ueura, B. Kawakami, T. Hatakeyama, *Org. Lett.* **2020**, *22*, 700.
[58] K. Schickedanz, T. Trageser, M. Bolte, H.-W. Lerner, M. Wagner, *Chem. Commun.* **2015**, *51*, 15808.
[59] E. Nestoros, M. C. Stuparu, *Chem. Commun.* **2018**, *54*, 6503.
[60] J. Mack, P. Vogel, D. Jones, N. Kaval, A. Sutton, *Org. Biomol. Chem.* **2007**, *5*, 2448.
[61] Y.-C. Cheng, X. Tang, K. Wang, X. Xiong, X.-C. Fan, S. Luo, R. Walia, Y. Xie, T. Zhang, D. Zhang, J. Yu, X.-K. Chen, C. Adachi, X.-H. Zhang, *Nat. Commun.* **2024**, *15*, 731.
[62] Y. Kondo, K. Yoshiura, S. Kitera, H. Nishi, S. Oda, H. Gotoh, Y. Sasada, M. Yanai, T. Hatakeyama, *Nat. Photonics* **2019**, *13*, 678.
[63] M. Mamada, M. Hayakawa, J. Ochi, T. Hatakeyama, *Chem. Soc. Rev.* **2024**, *53*, 1624.
[64] J. Ochi, Y. Yamasaki, K. Tanaka, Y. Kondo, K. Isayama, S. Oda, M. Kondo, T. Hatakeyama, *Nat. Commun.* **2024**, *15*, 2361.
[65] E. Fresta, J. Dosso, J. Cabanillas-Gonzalez, D. Bonifazi, R. D. Costa, *ACS Appl. Mater. Interfaces* **2020**, *12*, 28426.
[66] S. Tang, Y. Tsuchiya, J. Wang, C. Adachi, L. Edman, *Nat. Commun.* **2025**, *16*, 653.
[67] M. Chen, J. Ye, J. Lu, S. Wu, G. Lin, Y. Ma, L. Liu, Y. Zhang, L. Niu, B. Zhang, *Org. Electron.* **2025**, *142*, 107252.
[68] J. Wang, H. Hafeez, S. Tang, T. Matulaitis, L. Edman, I. D. W. Samuel, E. Zysman-Colman, *Aggregate* **2024**, *5*, 571.
[69] S. Tang, J. M. dos Santos, J. Ràfols-Ribé, J. Wang, E. Zysman-Colman, L. Edman, *Adv. Funct. Mater.* **2023**, *33*, 2306170.
[70] H. T. Ang, A. A. Ponich, M. Paladino, M. Miskolzie, D. G. Hall, *J. Am. Chem. Soc.* **2022**, *144*, 10570.
[71] S. Yruegas, J. J. Martinez, C. D. Martin, *Chem. Commun.* **2018**, *54*, 6808.
[72] W. Zhang, G. Li, L. Xu, Y. Zhuo, W. Wan, N. Yan, G. He, *Chem. Sci.* **2018**, *9*, 4444.
[73] K. D. Harris, B. M. Kariuki, C. Lambropoulos, D. Philp, J. M. Robinson, *Tetrahedron* **1997**, *53*, 8599.
[74] D. Stassen, N. Demitri, D. Bonifazi, *Angew. Chem., Int. Ed.* **2016**, *55*, 5947.
[75] J. L. Bricks, Y. L. Slominskii, I. D. Panas, A. P. Demchenko, *Methods Appl. Fluoresc.* **2017**, *6*, 012001.
[76] V. Jankus, K. Abdullah, G. C. Griffiths, H. Al-Attar, Y. Zheng, M. R. Bryce, A. P. Monkman, *Org. Electron.* **2015**, *20*, 97.
[77] S. B. Meier, D. Tordera, A. Pertegás, C. Roldán-Carmona, E. Ortí, H. J. Bolink, *Mater. Today* **2014**, *17*, 217.
[78] J. Ràfols-Ribé, X. Zhang, C. Larsen, P. Lundberg, E. M. Lindh, C. T. Mai, J. Mindemark, E. Gracia-Espino, L. Edman, *Adv. Mater.* **2022**, *34*, 2107849.
[79] S. Jenatsch, M. Regnat, R. Hany, M. Diethelm, F. Nüesch, B. Ruhstaller, *ACS Photonics* **2018**, *5*, 1591.
[80] S. Jha, R. Haroldson, A. A. Zakhidov, J. D. Slinker, *M. R. S. Commun.* **2024**, *14*, 196.
[81] G.-R. Lin, H.-F. Chen, H.-C. Shih, J.-H. Hsu, Y. Chang, C.-H. Chiu, C.-Y. Cheng, Y.-S. Yeh, H.-C. Su, K.-T. Wong, *Phys. Chem. Chem. Phys.* **2015**, *17*, 6956.
[82] N. Kaihovirta, A. Asadpoordarvish, A. Sandström, L. Edman, *ACS Photonics* **2014**, *1*, 182.
[83] N. Kaihovirta, G. Longo, L. Gil-Escrig, H. J. Bolink, L. Edman, *Appl. Phys. Lett.* **2015**, *106*, 103502.
[84] S. M. Suresh, D. Hall, D. Beljonne, Y. Olivier, E. Zysman-Colman, *Adv. Funct. Mater.* **2020**, *30*, 1908677.